Research Article | Vol. 31, No. 22 / 23 Oct 2023 / Optics Express 36824
Optics EXPRESS

Amplitude noise suppression in Yb:doped NALM oscillators utilizing saturable absorber settings

VITO F. PECILE,[1,2,*] ALINE S. MAYER,[1] JONAS K. C. BALLENTIN,[1] AND OLIVER H. HECKL[1]

[1] University of Vienna, Faculty of Physics, Faculty Center for Nano Structure Research, Christian Doppler Laboratory for Mid-IR Spectroscopy, Boltzmanngasse 5, 1090 Vienna, Austria
[2] University of Vienna, Vienna Doctoral School in Physics, Boltzmanngasse 5, 1090 Vienna, Austria
[*] vito.pecile@univie.ac.at

Abstract: Optical frequency combs based on fiber lasers mode-locked (ML) with a nonlinear amplifying loop mirror (NALM) have become the backbone of many cutting-edge applications, ranging from precision spectroscopy to quantum physics. Being extremely precise measurement tools, understanding their passive stability and low-noise operation regimes is vital. While several influences on the laser noise have been studied, many parameters remain poorly understood. Here, we systematically analyze under which preconditions the artificial saturable absorber settings of the laser can be modified during operation without losing mode-locking and the effects on laser noise, the spectrum and the output power. Our results show that it is possible to decrease the amplitude noise (AM noise) of the laser by more than 50 % by simply rotating a wave plate within the laser cavity. Additionally, we discuss differences to a similar effect observed in a NALM-alike laser amplifier and of changing the output coupling. These findings deepen our understanding and capabilities of optimizing the noise performance of ML fiber lasers, enable us to investigate new parameter spaces, and can be used to further optimize the noise performance of the NALM laser design, making it an ideal light source for advanced setups both in research and industry.

1. Introduction

Over the past few years, the interest in low-noise ML fiber lasers has increased tremendously [1,2]. Many applications, among them, precision spectroscopy [3], frequency metrology [4], breath analysis for disease detection [5], or trace gas sensing [6], rely on robust, reliable, and easy-to-operate laser sources. A common technique to achieve mode-locking in fiber lasers is nonlinear polarization evolution (NPE) [7], using standard single mode (SM) fibers. This technique suffers from poor stability, as lasers using SM fibers are known for being prone to environmental perturbations. Introducing polarization-maintaining (PM) fibers resulted in increased robustness. However, to be able to use them with NPE, complicated techniques such as cross-splicing are necessary [8]. A simpler and more versatile laser design using PM fibers is the so called NALM [9–11], which uses a Sagnac loop as an artificial saturable absorber to mode-lock the laser, which, in contrast to a real saturable absorber, does not degrade over time. A laser ML with a NALM can be built with off-the-shelf components, which are readily available and low-cost. Additionally, the laser parameters can be easily tailored to the user's needs, making the NALM mode-locking technique an ideal candidate for many cutting-edge applications. Since the first introduction of this type of laser [12,13], various publications have shown progress in, e.g., power scaling [14,15], frequency comb stabilization [16], or single-cavity dual-comb schemes [17,18], showing high interest and activity in the scientific community.

#501997 https://doi.org/10.1364/OE.501997
Journal © 2023 Received 31 Jul 2023; revised 13 Sep 2023; accepted 23 Sep 2023; published 17 Oct 2023

Optics EXPRESS

Due to their excellent low-noise properties [10,19], NALM based lasers have become the backbone of many metrology and spectroscopy systems that rely on optical frequency combs as a stable light source. Therefore, a particular interest of the research community in the past few years has been to further understand and optimize the noise behavior of that laser type as well as to identify operational regimes which show optimal noise properties. An important and well-understood aspect when it comes to the noise performance of any laser is the total intra-cavity GDD. Theoretical predictions from the 1990s that the noise of lasers is minimal, when it is operated around zero intra-cavity GDD, i.e., the stretched pulse regime [20], have been verified for several types of lasers and also been studied in great detail for NALM oscillators both for Erbium and Ytterbium based systems. For example, Mayer et al. [11] have demonstrated that in an Yb:doped NALM laser the operational states with the best noise performance can be found around slightly negative, close-to-zero total intracavity GDD, reaching root mean square relative intensity noise (RMS RIN) values among the best state-of-the-art free-running lasers [10]. Hutter et al. [21] have recently investigated the carrier-envelope offset (CEO) frequency linewidths and phase noise properties of different Er:doped NALM oscillators, reaching CEO linewidths below 1 kHz at +1100 fs^2 intracavity GDD. They also identify ideal pump powers to minimize laser noise. Another parameter that is known to influence the laser noise is the laser cavity losses. It has been shown in NPE lasers, that the laser RIN scales with the laser losses, i.e., higher laser output powers come at the cost of worse RIN performance, when increasing the output coupling ratio [22]. Note, that to the best of our knowledge, this study has not yet been repeated for NALM lasers.

Apart from using dispersion, pump power and the cavity output coupling rate as a means to optimize the laser noise performance, many mechanisms that could have an effect on the noise properties of NALM lasers are not well understood yet and still lack investigation. A relatively new approach is to utilize the settings of the NALM based artificial saturable absorber (NALM-ASA) not only to achieve (self-starting) ML operation of the laser, but also to suppress the laser amplitude noise. In general, in a NALM oscillator the phase bias and the modulation depth of the NALM-ASA can be changed with the help of polarization optics, i.e., the rotation state of wave plates inside the laser cavity. The challenge here is that for most operational states already slight changes of the NALM-ASA settings result in a loss of ML operation, as in general the pulse shaping mechanisms inside the cavity are very sensitive to changes of the NALM-ASA settings [10]. To still be able to investigate the noise behavior of a NALM loop based on the NALM-ASA settings, Edelmann et al. [23] decoupled the NALM loop from the oscillator dynamics by amplifying the pulses of an external seed laser, forming a NALM-alike laser amplifier. They investigated the laser RIN and found a suppression effect, based on the setting of the phase bias of the NALM-ASA. In a different publication, the same authors also utilize changes in the modulation depth of the laser to design a laser amplification scheme based on a NALM [24]. However, the authors explicitly state that they were not able to directly investigate that effect in-situ in a NALM laser, as they lost ML operation due to the above discussed instability issues for already subtle NALM-ASA changes. Therefore, the NALM-ASA settings can not yet be utilized to tune the laser noise, and an investigation of this suppression effect in a NALM oscillator is still lacking in literature.

In the here presented work, we investigate, whether operational states exist in a NALM laser, where a change of the NALM-ASA parameters is possible without the loss of ML operation so that we can directly investigate the noise behaviour of the laser. To do so, we mode-locked the laser in different dispersion regimes, ranging from soliton, to stretched pulse, and all normal dispersion (ANDi). We can confirm that in most cases ML operation is indeed lost already with slight NALM-ASA changes. A tuning of the modulation depth was not possible in any case without losing mode-locking. This is the case as to induce and maintain mode-locking in a NALM oscillator, it is necessary to set the modulation depth close to the maximal possible value.

Optics EXPRESS

The behavior is different in the case of the phase bias of the NALM-ASA. We could identify that in the stretched pulse dispersion regime – which also shows the best noise performance based on intracavity GDD [11,20] – tuning the phase bias is possible over a wide parameter range without losing clean ML operation. This allows for a systematic investigation of the AM noise suppression effect based on the laser phase bias in situ, while continuously operating the laser in a clean ML state. We analyze the RMS RIN performance as well as changes in the output power and the optical spectrum of the laser at both laser output ports for different phase bias settings. We identify laser operating states with the best AM noise performance, changes in output power, as well as spectral changes, and discuss differences to the suppression effect reported in a NALM-alike laser amplifier [23]. Our results show clearly that it is possible to reduce the amplitude noise compared to the self-starting laser configuration by changing the phase bias of the NALM-ASA, suppressing the integrated RMS RIN by more than a factor of two in a Fourier frequency range of [1 Hz, 10 MHz]. The favorable laser state not only shows an optimized AM noise performance, but also features a more broadband optical spectrum, as well as higher average power at the output port of the oscillator.

Also, we investigate the dependency of the laser RIN on the laser losses by changing the output coupling rate. We see the same effect as reported for NPE lasers [22], i.e., increased output losses also increase the RIN of the laser. This makes utilizing the NALM-ASA noise suppression effect even more attractive, as we additionally increase the laser output power without the need of changing the linear losses of the laser and therefore reach a superior AM noise performance and achieve higher output powers simultaneously.

2. Laser and measurement setup

2.1. Laser setup and properties

The investigated laser consists of an all polarization-maintaining (PM) fiber section, which forms a NALM loop by asymmetrically placing an Yb:doped gain fiber between two single-mode fibers. Pump light from a laser diode emitting at 976 nm enters it via a wave-division multiplexer (WDM). The loop is completed by splicing the two open fiber ends to a polarizing beam-combining collimator (PBCC). Light which enters the PBCC gets split into two orthogonally polarized waves propagating in opposite directions through the loop. Due to the asymmetrical placement of the active fiber, the two waves see a different nonlinear phase shift, which leads to a phase shift difference $\Delta\phi$ when the two waves are recombined at the PBCC. More intracavity transmission is achieved for higher $\Delta\phi$ and therefore higher peak intensities, favouring ML over CW operation. The free-space section features a transmission grating pair for flexible intracavity GDD management, a rotatable half-wave plate (HWP) θ_o in combination with a polarizing beam cube (PBC) for the management of the output coupling, and a Faraday rotator (FR) as well as a rotatable HWP θ_h and quarter-wave plate (QWP) θ_q to add a nonreciprocal phase bias and to change the behavior of the NALM-ASA. The parameters θ_i represent the angles between the fast axis of the wave plates and a reference axis and therefore the rotation state of the respective wave plates. We use the same reference axis definition as in [11], where the axis is parallel to the optical table and normal to the beam propagating in the free-space section of the cavity, coming from the PBCC. A silver mirror is used to close the cavity. The laser has two ports where light is coupled out of the cavity, one usually referred to as output-, transmission- or T-port, and a second one called rejection- or R-port. In most applications the T-port light is preferred over the R-port output. This is due to the fact that the spectral wings of the light wave coming from the NALM loop get coupled out at the R-port, leading to disturbed spectra and worse noise performance, while at the same time cleaning the spectrum exiting the cavity at the T-port. However, the R-port can be used for several applications in parallel to the T-port, e.g., for seeding an f-to-2f interferometer for CEO stabilization. A scheme of the setup is shown in Fig. 1(a). The laser operates at a repetition rate of about 77 MHz and delivers 1 ps long 200 pJ pulses with a central

Optics EXPRESS

wavelength of 1060 nm. We use the exact same oscillator as in [11], where a detailed description of the oscillator, including part lists and exact measures of all fiber bits, can be found.

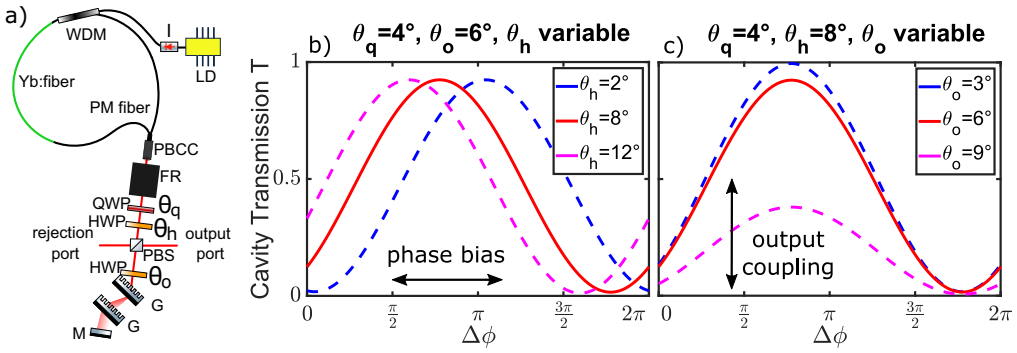

Fig. 1. **(a)** Scheme of the laser: LD, laser diode; I, isolator; WDM, wavelength division multiplexer; Yb:fiber, Yb doped gain fiber; PM fiber, polarization-maintaining fiber; PBCC, polarizing beam-combining collimator; FR, Faraday rotator; HWP, half-wave plate; QWP, quarter-wave plate; G, transmission grating; M, silver mirror; θ_o, θ_h and θ_q, rotation states of wave plates. **(b)** Cavity transmission function $\mathbf{T}(\Delta\phi)$ for $\theta_q = 4°, \theta_o = 6°$ and different θ_h. $\theta_h = 8°$ corresponds to self-starting ML operation. **(c)** Cavity transmission function $\mathbf{T}(\Delta\phi)$ for $\theta_q = 4°, \theta_h = 8°$ and different θ_o. $\theta_o = 6°$ corresponds to self-starting ML operation.

2.2. *Laser cavity transmission function and mode-locking parameters*

To establish a connection between the rotation states of the wave plates within the laser cavity and the thereby changed laser parameters, it is useful to calculate the so-called cavity transmission function $\mathbf{T}(\Delta\phi, \theta_o, \theta_h, \theta_q)$. To calcuate $\mathbf{T}(\Delta\phi, \theta_o, \theta_h, \theta_q)$, the Jones matrices [25] for all polarization optics within the laser cavity are added up until we reach the same point within the cavity again, modelling the change of the polarization within the cavity over a full roundtrip. Normalizing the intensity of the light within the cavity to the total intensity (light resonant inside the cavity and the intensity of the light coupled out at the T- and R-ports), we receive the cavity transmission function. With the same method, it is also possible to model the linear and the saturable losses of the laser. For a detailed description and calculation of the cavity transmission function, we refer to [11].

As the rotation states θ_i can be easily obtained from the setup, they are usually fixed to concrete values, and the cavity transmission function reduces to $\mathbf{T}(\Delta\phi)$, which can be more easily visualized and interpreted. By plotting $\mathbf{T}(\Delta\phi)$ for variations of θ_i a clear connection between the wave plate rotation and the associated laser property can be made. The simplified cavity transmission function for variations of θ_h and θ_o is given in Figs. 1(b) and (c), respectively. We now see that a change in θ_h refers to the phase bias in the cavity, while θ_o is linked to the laser output coupling rate, i.e., the linear losses. θ_q changes the modulation depth of the laser. However, we did not show variations of θ_q, as this parameter remains unchanged in our study.

To mode-lock the laser in a self-starting configuration, it is necessary to find a set of rotation states for θ_o, θ_h and θ_q that results in ML operation just by increasing the pump power. It is necessary to adjust the phase bias of the laser in a way, that the cavity transmission increases for higher $\Delta\phi$, i.e., is on the rising slope for $\Delta\phi = 0$. In most cases, it is also beneficial to have low linear losses as well as a large modulation depth. This allows for a steep $\mathbf{T}(\Delta\phi)$, making ML operation attractive for the laser. The transmission function that we used for self-starting mode-locking of our laser is shown as red curve in Fig. 1(b). An algorithm which can be used to achieve mode-locking in NALM lasers is given in [11].

Optics EXPRESS

2.3. Measurement setup

To investigate the effect of different phase bias settings on the laser RIN, we rotated θ_h, as shown in Fig. 1(b). As a first step, we identified the lower ($\theta_{h,\,min}$) and upper bound ($\theta_{h,\,max}$) which still ensure clean ML operation. In a second step, for every set of laser parameters, systematic measurements of average power, AM noise, and the optical spectrum were performed for equidistant points with a spacing of 1° at both the T- and the R-port. The power measurements were done with a thermal power sensor (Thorlabs S302C), to be insensitive to spectral changes throughout a measurement series.

The AM noise and the RF traces were measured using a Thorlabs DET08CL InGaAs photodetector (PD) with 5 GHz bandwidth in combination with a Rohde & Schwarz FSWP8 Phase Noise Analyzer (PNA). Fast PDs have a very small optical area, therefore we used a tightly focused, highly attenuated beam to avoid beam-pointing issues as well as an early saturation of the PD. To ensure comparable results, all measurements were performed with the same alignment of the PD, as we have seen that already small alignment changes can lead to different results in the measured laser noise. This is due to illuminating another part of the optical area of the PD with slightly different response, caused by material inhomogeneities or by a small tilt of the beam relative to the detector surface.

All noise measurements performed with the PNA were done at the laser repetition rate as a carrier frequency and at the same carrier power (-20 dBm). The measurements presented in Fig. 2(a) were measured with 2000 cross-correlations (XCORR) and a resolution bandwidth (RBW) of 1 % to receive flat measurement curves with high Fourier frequency resolution. All other measurements shown in Fig. 2(c) were measured with 20 XCORR and a RBW of 5 % to allow for faster data acquisition. This was possible without trading-off on the quality of the received measurement data, as the lower RBW and XCORR average out when integrating the AM noise data to receive the RMS RIN, leading to the same results as when using higher settings. In all cases the power spectral density (PSD) of the intensity noise $S_a(f)$ was measured in single-sideband (SSB) mode in the Fourier frequency range of [1 Hz, 10 MHz]. We then receive the RMS RIN specified in % by using the relation

$$\frac{\delta P}{\overline{P}}|_{RMS} = 100\sqrt{2\int_{1\text{ Hz}}^{10\text{ MHz}} S_a(f)\,\mathrm{d}f}\ .$$

The optical spectra were obtained with an Ando AQ6315A optical spectrum analyzer.

We also investigated, whether the change in RIN has an effect on the phase noise performance of the oscillator. Therefore, we measured the phase noise at the 15th harmonic of the repetition rate for several points between $\theta_{h,\,min}$ and $\theta_{h,\,max}$ and compared the results. Apart from that, we used the same measurement procedure and settings as described above for the AM noise measurements.

Additionally, to study the effect of changing the linear losses of the laser on the RIN performance, we rotated θ_o, as shown in Fig. 1(c). Here, analog to the investigation of changes in θ_h, we also identified the lower and upper bound for which clean ML operation was given and performed AM noise/RMS RIN measurements with the same setup and settings as described above.

Optics EXPRESS

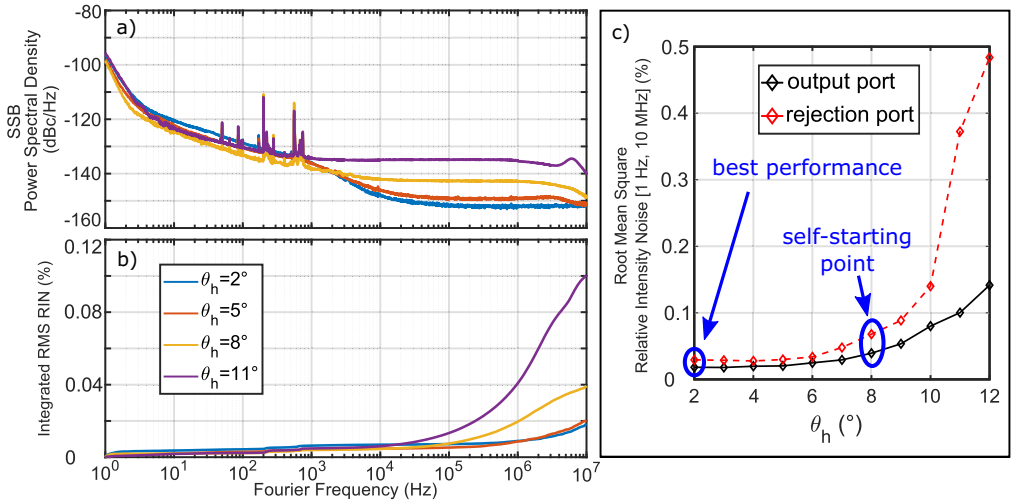

Fig. 2. **(a)** SSB AM noise power spectral density for exemplary settings of θ_h, measured at the output port. **(b)** Cumulative integration of the above shown AM noise measurements to calculate the RMS RIN with variable cut-off frequencies. **(c)** RMS RIN values for the whole investigated range of Fourier frequencies, [1 Hz, 10 MHz].

3. Analysis of the effects for changes in the NALM-ASA settings

In our investigation we were able to find several laser states around zero intracavity GDD that supported self-starting mode-locking and allowed for a change in θ_h as well as θ_o. The different laser states were accessed by slightly tuning the distance between the grating pair and therefore changing the intracavity GDD. In all cases, a complete set of data was recorded, showing consistent trends for all presented laser properties. The state with the largest tuning range was found at a grating distance $d = 8.17$ mm, which corresponds to an intra-cavity GDD of roughly $0.015\,\text{ps}^2$ at 1030 nm and $-0.01\,\text{ps}^2$ at 1080 nm and is discussed exemplarily in this work. A detailed discussion on how to measure the intracavity GDD for the given laser is found in [11]. For the state presented in our manuscript, we directly switch on the laser pump diode with an optical power of 120 mW and immediately achieve single-pulsed operation without any further necessary modification of the pump power. The pump power is then kept stable throughout the whole measurement series. The waveplate settings for the self-starting operation were $\theta_h = 8°$, $\theta_o = 6°$ and $\theta_q = 4°$. The range in which the laser was operated without losing mode-locking is given by $\theta_{h,max} = 12°$ and $\theta_{h,min} = 2°$. The transmission function repeats periodically every 45° for a change in θ_h. As a positive slope is required for mode-locking, the theoretically possible tuning range reduces to 22.5°. A change of 10° (i.e. 2° to 12°) therefore represents almost half of the theoretically possible phase bias settings.

As already briefly mentioned in the introduction, all laser states proved to be very sensitive to changes in θ_q, i.e., a change in the modulation depth, already losing ML operation for minimal changes. Note that tuning of this second NALM-ASA parameter is however used for noise suppression and amplification in a nonlinear fiber system [24], similar to the one reported in [23].

3.1. Changes in the laser noise

Our analysis of the AM noise measurements for varying θ_h is depicted in Fig. 2. One can see that the RMS RIN increases significantly for both ports when increasing θ_h. The best noise performance can be found for the lowest possible settings of θ_h for both ports. The output port clearly outperforms the rejection port over the whole investigated range of θ_h (see Fig. 2(c)).

Optics EXPRESS

We see a different behavior than observed for the NALM-alike amplifier, where an opposite monotonicity for the two laser ports for variations of θ_h was reported [23], which allowed for states, were the rejection port noise performance was superior to the output port.

The following analysis focuses on the output port of the laser, as its noise properties are always superior to the rejection port and our goal is to identify the operation regime with the best noise performance. Looking at the AM noise measurements (see Fig. 2(a)), we observe a similar performance of all states for low Fourier frequencies of up to 1 kHz, and clear differences in the behavior for higher Fourier frequencies, where we see a difference of up to almost 20 dB in the SSB PSD, comparing the states for high and low θ_h. When cumulatively integrating the RMS RIN (see Fig. 2(b)), one can observe that the major contribution to the performance difference of the RMS RIN occurs in the Fourier frequency range above 20 kHz. This is highly beneficial, as the main improvement is in a Fourier frequency range that is larger than the bandwidth of most actuators that can be used to actively stabilize the laser intensity with a phase-locked loop (PLL) and can therefore only be improved passively by design or a smart choice of laser parameters. This noise behavior is similar to the results for a NALM-alike amplifier system [24]. In that work, the main RIN suppression that could be achieved was also in the area of higher Fourier frequencies and reached similar suppression levels. For settings of $\theta_h \leq 5°$ the RMS RIN begins to converge towards a minimal value, and the AM noise reduction per degree of change in θ_h becomes very small.

We also investigated whether we could observe changes in the phase noise. It is well known that the RIN couples to the phase noise of an oscillator by different effects, e.g., via self-steepening or Gordon-Haus jitter [2,26]. Those effects dominate at low Fourier frequencies, where we do not see a substantial change in the AM noise. Therefore, we did not observe any changes in the phase noise behavior of the laser.

To optimize the laser noise performance it is always necessary to perform parameter changes after self-starting mode-locking. In our case, we self-start the laser at $\theta_h = 8°$ and then rotate the wave plate to the minimal possible value that still allows for clean ML operation ($\theta_h = 2°$). This algorithm has shown to be extremely reliable (at the time of writing the manuscript it has been repeated several hundred times without a single issue) and the resulting noise-optimized state is very stable (no loss of ML operation for more than half a year of uninterrupted operation). To ensure clean ML operation, we constantly monitored the RF trace of the laser as well as the spectrum for any modulations or disturbances. Measured RF traces for our noise-optimized laser state with $\theta_h = 2°$ are shown exemplarily in Fig. 3(c) and (d).

3.2. Changes in optical spectrum and output power

We observed that the changes in noise performance for different θ_h are accompanied by a change in the optical spectrum and in the measured output power of the laser ports. In the self-starting configuration (red curve in Fig. 3(a)), we see that our spectrum consists of a main peak at 1060 nm, where almost all of the optical power is located, and a small side peak at 1030 nm. It is important to note that these small side peaks are characteristic for laser states with slightly-negative, close-to-zero intracavity GDD, i.e., in the stretched pulse regime [11]. When minimizing θ_h, the two distinct peaks begin forming a single broadband pulse shape, with a plateau between 1030 nm to 1040 nm (blue dashed curve in Fig. 3(a)). Further decreasing the parameter leads to a CW-breakthrough. On the contrary, by increasing θ_h the two peaks become more distinct and an increasing amount of optical power is located at the 1030 nm peak (magenta dashed curve in Fig. 3(a)). Increasing θ_h further leads to multi-pulsing in the laser. Although the spectrum for $\theta_h = 12°$ looks very similar to what one would expect to be a CW breakthrough, this is not the case. Those occur at a different wavelength (1040 nm) and are narrower.

Looking at the changes in average power, we see a monotonic decrease with θ_h (see Fig. 3(b)). We see an increase in average power of 25 %, comparing 15.4 mW at the self-starting configuration

Optics EXPRESS

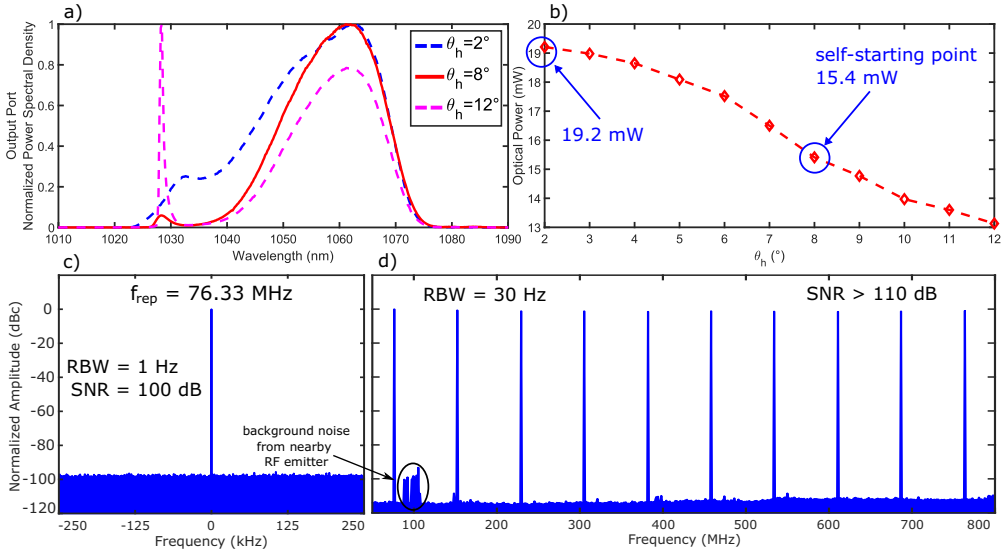

Fig. 3. **(a)** Spectral changes for variations of θ_h at the output port. $\theta_h = 8°$ is the spectrum for self-starting ML operation, $\theta_h = 2°$ and 12° are the measured spectra for the lowest and highest settings, respectively. **(b)** Changes of average power at the output port for variations of θ_h. The power decreases monotonically with θ_h. The output power is increased by 25 % for $\theta_h = 2°$ compared to the self-starting configuration. **(c)** 500 kHz-spanned zoom into the first harmonic of the laser repetition rate with a resolution bandwidth (RBW) of 1 Hz and an achieved signal-to-noise ratio (SNR) of 100 dB for the noise-optimized laser state with $\theta_h = 2°$. **(d)** Wide span showing the first ten harmonics of the laser repetition rate with a RBW of 30 Hz and a SNR larger than 110 dB for the noise-optimized laser state with $\theta_h = 2°$. Note, that the indicated noise at roughly 100 MHz is unavoidable background noise that does neither come from the laser nor the used PD.

to the minimal setting of θ_h, where an average power of 19.2 mW was observed at the output port. We simultaneously measured the output power at the rejection port. The overall output power of the laser at both ports was relatively stable over the whole investigated range of θ_h. Therefore, by increasing the power at the output port we decreased the power at the rejection port by roughly the same amount.

An overview of the laser output power, the spectral full width at half maximum (FWHM), and the integrated RMS RIN of the output port of the laser for variations of θ_h is given in Table 1.

3.3. *Discussion of the laser behavior*

A possible explanation of the observed noise suppression is that the laser compensates the losses inflicted by the change of the phase bias by shifting the spectrum towards a wavelength region with more gain, which also explains the observed spectral changes. We calculated that the working point of the laser in terms of $\Delta\phi$, which is located at the rising slope of the cavity transmission function, only changes marginally with θ_h after mode-locking the laser. This estimation can be made, as the difference in energy splitting ratio k is only 1.17 % for the full range of our investigation of θ_h (2° to 12°). We used the same calculation method for k as presented in [11]. Using $\Delta\phi \propto (1-k)/k$, which follows from [23], we see that the total change in $\Delta\phi$ is calculated as 2.8 %. This means that a change in phase bias (by rotating θ_h) translates directly into a change in cavity transmission (see Fig. 1(b)). For lower values of θ_h we now reduce the cavity transmission and the laser compensates for the inflicted losses by shifting parts of the spectrum towards

Optics EXPRESS

Table 1. Average power, FWHM and RMS RIN values of the output port for variations of θ_h. For $\theta_h = 12°$ the peak at 1030 nm is stronger than the one at 1060 nm (see Fig. 3 (a)). However, for a senseful comparison with the other states we present the FWHM for the peak at 1060 nm. The self-starting setting is given for $\theta_h = 8°$.

θ_h	Average Power	FWHM	RMS RIN [1 Hz, 10 MHz]
2°	19.2 mW	24.1 nm	0.018 %
3°	19.0 mW	22.7 nm	0.018 %
4°	18.7 mW	22.2 nm	0.020 %
5°	18.1 mW	21.5 nm	0.020 %
6°	17.5 mW	20.9 nm	0.025 %
7°	16.5 mW	20.4 nm	0.029 %
8°	15.4 mW	19.9 nm	0.039 %
9°	14.8 mW	19.5 nm	0.054 %
10°	14.0 mW	19.2 nm	0.080 %
11°	13.6 mW	18.9 nm	0.100 %
12°	13.1 mW	18.8 nm	0.142 %

the gain maximum of Ytterbium at shorter wavelengths (see Fig. 3(a)), minimizing amplified spontaneous emission, which is wavelength dependent and occurs around 1030 nm, and therefore the RIN.

As a follow-up study to our work it would be interesting to investigate wavelength dependent noise phenomena by utilizing spectral filters outside the laser cavity. This would allow to investigate whether specific noise phenomena could be in fact associated with a certain wavelength region and lead to a potential verification of our above made explanations.

The results we obtain are different from those of the NALM-alike laser amplifier presented in [23]. For the here presented NALM oscillator, the output port always has lower RMS RIN than the rejection port. Both ports also show the same monotonicity for changes in θ_h in terms of RMS RIN. This stands in contrast to the NALM-alike laser amplifier, where a reciprocal monotonicity has been observed and states exist, where the rejection port is superior to the output port. While in the case of the NALM-alike amplifier a single round-trip in the NALM-loop is emulated, we do an in-situ investigation of an actual laser oscillator. This adds laser oscillator dynamics and also includes aspects of, e.g., intracavity GDD, pulse-shaping inside the cavity, or the above discussed wavelength-dependent gain-loss aspects. Altogether, this leads to the observation of a different behavior.

4. Noise analysis for different output coupling rates

Additionally, we investigated the changes in RMS RIN when changing the output coupling of the laser by rotating θ_o. Here, the range in which the laser was operated without losing mode-locking is given by $\theta_{o,\,max} = 9°$ and $\theta_{o,\,min} = 2°$. The analysis of the RMS RIN at the output port for varying θ_o is shown in Fig. 4(b). The same laser parameters were used as for the earlier analysis of θ_h. We found that increasing θ_o does not only result in higher output powers (see Fig. 4(a)), but also leads to higher RMS RIN. This observation agrees with the results obtained for an NPE laser [22]. Looking at Fig. 4(c), we see, that major differences in AM noise occur for lower Fourier frequencies in the range of [15 Hz, 7 kHz] while the results for the other Fourier frequency regions are similar. The overall contribution of this region to the total integrated RMS RIN however is not substantial, as differences in the other Fourier frequency regions contribute more to the overall result, which is clearly visible when looking at the iterative integrals shown in Fig. 4(d). The best RMS RIN performance can be found for the highest intracavity power.

Optics EXPRESS

If higher output powers are needed, it is a better alternative to first minimize θ_h, as this also increases the power at the output port and allows for a better RMS RIN performance, as discussed above and shown in Fig. 3(b). By using θ_h to increase the power levels, we were able to reach 80 % of the maximal output power that could have been achieved by changing θ_o while at the same time improving 60 % on the RIN performance in the observed Fourier frequency range. It is only necessary to also change θ_o if even higher output powers are needed.

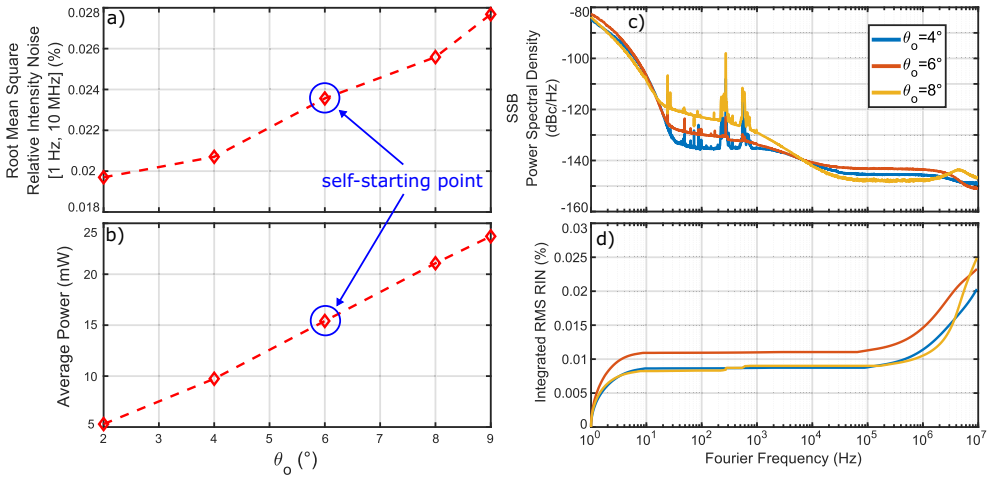

Fig. 4. **(a)** Integrated RMS RIN at the output port for variations of θ_o. **(b)** Changes of the average power for variations of θ_o at the output port. Increasing the output power by rotating θ_o comes at the cost of a worse RMS RIN performance. **(c)** SSB AM noise measurements for variations of θ_o. **(d)** Cumulative integration of the above shown AM noise measurements to calculate the RMS RIN with variable cut-off frequencies.

In contrast to θ_h, no significant spectral changes were observed when changing θ_o. Measuring the phase noise for different θ_o, we could not see any relevant performance differences. This is consistent with the explanation given for the phase noise performance in the case of tuning the phase bias above.

It is also possible to use both wave plates to optimize the AM noise performance of the laser. We see, that for θ_h the potential to reduce the RMS RIN is greater than 50 % while for θ_o the potential is only roughly 20 %. Therefore, an ideal strategy is to first minimize θ_h and to subsequently also minimize θ_o, which then has a slightly reduced tuning range.

5. Conclusion

We have investigated the noise performance of an Yb-doped all-PM ML NALM laser oscillator in dependence of its NALM-ASA settings, i.e., the rotation states of the wave plates within the laser cavity. Tuning the wave plates over a wide range without losing ML operation is possible in the close-to-zero total intracavity GDD (i.e., stretched pulse) regime, which is known for the lowest-noise states for this type of laser. We have shown that a reduction of the RMS RIN performance by more than 50 % is possible, compared to the self-starting ML operation state of the laser. The main suppression occurs at high Fourier frequencies which can not be actively stabilized due to the limited bandwidth of available actuators, making the laser more intrinsically stable in an otherwise inaccessible region.

The lowest AM noise can be found for the largest phase bias settings of the NALM-ASA. The output port always outperforms the rejection port. Both show the same monotonicity for changes in θ_h in terms of RMS RIN. A reciprocal monotonicity of the RMS RIN of the output

Optics EXPRESS

and the rejection port, as demonstrated for a NALM-alike amplifier [23], could not be observed. Accompanying changes in the laser output spectrum as well as the average power have been analysed and discussed, showing an increase in laser average power of 25 % and a more broadband spectrum for the noise-optimized laser state.

Additionally, we have discussed the influence on the RMS RIN, when changing the laser output coupling by rotating θ_o, showing a noisier behavior for higher output powers. We thereby could confirm that lower linear losses minimize the laser RIN, which so far, to the best of our knowledge, has only been shown experimentally for NPE lasers [22].

The findings of this work can be used to fully utilize the potential of the NALM laser design, optimizing both the AM noise performance as well as the output power and tuning the optical spectrum, making the laser a very versatile, low-noise source as a master oscillator used in many cutting edge applications.

Funding. Österreichische Nationalstiftung für Forschung, Technologie und Entwicklung; Bundesministerium für Digitalisierung und Wirtschaftsstandort; Christian Doppler Forschungsgesellschaft; Austrian Science Fund (M 2561, P 33680, P 36040).

Acknowledgments. We thank Jakob Fellinger and P.E. Collin Aldia for valuable discussions. This research was funded in part by the Austrian Science Fund (FWF) [P 33680,P 36040, M 2561]. The financial support by the Austrian Federal Ministry for Digital and Economic Affairs, the National Foundation for Research, Technology and Development and the Christian Doppler Research Association is gratefully acknowledged.

Disclosures. VFP, ASM, JKCB, OHH: Thorlabs Inc. (F)

Data availability. Data underlying the results presented in this paper are not publicly available at this time but may be obtained from the authors upon reasonable request.

References

1. M. E. Fermann and I. Hartl, "Ultrafast fibre lasers," Nat. Photonics **7**(11), 868–874 (2013).
2. M. Endo, T. D. Shoji, and T. R. Schibli, "Ultralow Noise Optical Frequency Combs," IEEE J. Sel. Top. Quantum Electron. **24**(5), 1–13 (2018).
3. A. Marian, M. C. Stowe, J. R. Lawall, D. Felinto, and J. Ye, "United Time-Frequency Spectroscopy for Dynamics and Global Structure," Science **306**(5704), 2063–2068 (2004).
4. T. Udem, R. Holzwarth, and T. W. Hänsch, "Optical frequency metrology," Nature **416**(6877), 233–237 (2002).
5. M. Metsälä, "Optical techniques for breath analysis: from single to multi-species detection," J. Breath Res. **12**(2), 027104 (2018).
6. B. Nozière, M. Kalberer, and M. Claeys, *et al.*, "The Molecular Identification of Organic Compounds in the Atmosphere: State of the Art and Challenges," Chem. Rev. **115**(10), 3919–3983 (2015).
7. M. Hofer, M. E. Fermann, F. Haberl, M. H. Ober, and A. J. Schmidt, "Mode locking with cross-phase and self-phase modulation," Opt. Lett. **16**(7), 502–504 (1991).
8. Y. Wang, L. Zhang, Z. Zhuo, and S. Guo, "Cross-splicing method for compensating fiber birefringence in polarization-maintaining fiber ring laser mode locked by nonlinear polarization evolution," Appl. Opt. **55**(21), 5766–5770 (2016).
9. M. E. Fermann, F. Haberl, M. Hofer, and H. Hochreiter, "Nonlinear amplifying loop mirror," Opt. Lett. **15**(13), 752–754 (1990).
10. J. Kim and Y. Song, "Ultralow-noise mode-locked fiber lasers and frequency combs: principles, status, and applications," Adv. Opt. Photonics **8**(3), 465–540 (2016).
11. A. S. Mayer, W. Grosinger, J. Fellinger, G. Winkler, L. W. Perner, S. Droste, S. H. Salman, C. Li, C. M. Heyl, I. Hartl, and O. H. Heckl, "Flexible all-PM NALM Yb:fiber laser design for frequency comb applications: operation regimes and their noise properties," Opt. Express **28**(13), 18946–18968 (2020).
12. N. Kuse, J. Jiang, C.-C. Lee, T. R. Schibli, and M. Fermann, "All polarization-maintaining Er fiber-based optical frequency combs with nonlinear amplifying loop mirror," Opt. Express **24**(3), 3095–3102 (2016).
13. W. Hänsel, H. Hoogland, M. Giunta, S. Schmid, T. Steinmetz, R. Doubek, P. Mayer, S. Dobner, C. Cleff, M. Fischer, and R. Holzwarth, "All polarization-maintaining fiber laser architecture for robust femtosecond pulse generation," Appl. Phys. B **123**(1), 41 (2017).
14. W. Liu, H. Shi, J. Cui, C. Xie, Y. Song, C. Wang, and M. Hu, "Single-polarization large-mode-area fiber laser mode-locked with a nonlinear amplifying loop mirror," Opt. Lett. **43**(12), 2848–2851 (2018).
15. D. Duan, J. Wang, Y. Wu, J. Ma, and Q. Mao, "Approach to high pulse energy emission of the self-starting mode-locked figure-9 fiber laser," Opt. Express **28**(22), 33603–33613 (2020).
16. Y. Li, N. Kuse, A. Rolland, Y. Stepanenko, C. Radzewicz, and M. E. Fermann, "Low noise, self-referenced all polarization maintaining Ytterbium fiber laser frequency comb," Opt. Express **25**(15), 18017–18023 (2017).

Optics EXPRESS

17. R. Li, H. Shi, H. Tian, Y. Li, B. Liu, Y. Song, and M. Hu, "All-polarization-maintaining dual-wavelength mode-locked fiber laser based on Sagnac loop filter," Opt. Express **26**(22), 28302–28311 (2018).
18. J. Fellinger, A. S. Mayer, G. Winkler, W. Grosinger, G.-W. Truong, S. Droste, C. Li, C. M. Heyl, I. Hartl, and O. H. Heckl, "Tunable dual-comb from an all-polarization-maintaining single-cavity dual-color Yb:fiber laser," Opt. Express **27**(20), 28062–28074 (2019).
19. M. Giunta, M. Fischer, W. Hänsel, T. Steinmetz, M. Lessing, S. Holzberger, C. Cleff, T. W. Hansch, M. Mei, and R. Holzwarth, "20 Years and 20 Decimal Digits: A Journey With Optical Frequency Combs," IEEE Photonics Technol. Lett. **31**(23), 1898–1901 (2019).
20. S. Namiki and H. Haus, "Noise of the stretched pulse fiber laser. I. Theory," IEEE J. Quantum Electron. **33**(5), 649–659 (1997).
21. S. R. Hutter, A. Seer, T. König, R. Herda, D. Hertzsch, H. Kempf, R. Wilk, and A. Leitenstorfer, "Femtosecond Frequency Combs with Few-kHz Passive Stability over an Ultrabroadband Spectral Range," Laser Photonics Rev. **17**, 2200907 (2023).
22. I. L. Budunoglu, C. Ülgüdür, B. Oktem, and F. Ö. Ilday, "Intensity noise of mode-locked fiber lasers," Opt. Lett. **34**(16), 2516–2518 (2009).
23. M. Edelmann, Y. Hua, K. Safak, and F. X. Kärtner, "Intrinsic amplitude-noise suppression in fiber lasers mode-locked with nonlinear amplifying loop mirrors," Opt. Lett. **46**(7), 1752–1755 (2021).
24. M. Edelmann, Y. Hua, K. Safak, and F. X. Kärtner, "Nonlinear fiber system for shot-noise limited intensity noise suppression and amplification," Opt. Lett. **46**(14), 3344–3347 (2021).
25. R. C. Jones, "A New Calculus for the Treatment of Optical Systems I. Description and Discussion of the Calculus," J. Opt. Soc. Am. **31**(7), 488–493 (1941).
26. R. Paschotta, "Noise of mode-locked lasers (Part II): timing jitter and other fluctuations," Appl. Phys. B **79**(2), 163–173 (2004).